Forces on a sphere suspended in flowing granulate

Ralf Stannarius[1,2,*], *Jing* Wang[1], *Tivadar* Pongó[3], *Bo* Fan[4], *Tamás* Börzsönyi[4], and *Raúl Cruz* Hidalgo[3]

[1]Otto-von-Guericke-Universität Magdeburg, Magdeburg, Germany
[2]Technische Hochschule Brandenburg, Brandenburg an der Havel, Germany
[3]Universidad de Navarra, Pamplona, Spain
[4]HUN-REN Wigner Research Centre for Physics, Budapest, Hungary

Abstract. We investigate the forces of flowing granular material on an obstacle. A sphere suspended in a discharging silo experiences both weight of the overlaying layers and drag of the surrounding moving grains. In experiments with frictional hard glass beads, the force on the obstacle was found to be practically flow-rate independent. In contrast, flow of nearly frictionless soft hydrogel spheres added drag forces which increased with the flow rate until reaching saturation at high flow speeds. The total force grew quadratically with the obstacle diameter in the soft, low friction material, while it grew much weaker, nearly linearly with the obstacle diameter, in the bed of hard, frictional glass spheres. In addition to the drag, obstacles embedded in the flowing hydrogel spheres experience a weight force from the top as if immersed in a hydrostatic pressure profile, but negligible counter-forces from below. In contrast, the frictional hard particles create a strong pressure gradient near the upper surface of the obstacle. Numerical simulations provide additional information that is difficult to access experimentally. They reproduce the experimental results and give hints for the origin of the different force contributions. The results have considerable practical importance for the discharge of storage containers with large objects suspended in flowing granular material.

1 Introduction

The redistribution of forces in granular beds is an intricate problem. In heaps, for example, it depends not only on the container geometry, but also on the deposition protocol [1, 2]. Inside storage containers, walls carry part of the load of the grains, which leads to a pressure saturation in the deeper layers [3, 4]. The situation becomes even more complex with internal flow. Typical objects studied in granular drag flow are spheres, rods or horizontal plates that are lifted or plunged in a grain bed at constant speed [5–11]. Drag forces were found to be velocity independent but increased with penetration depth.

Several experimental studies [12–16] and DEM simulations [15–17] considered drag forces on objects suspended in an emptying silo, including spheres, cylinders, disk-shaped plates, and cones. A velocity-independent drag force was found both in the experiments and the numerical studies. An experimental study of forces of a sphere suspended in a silo filled with soft and hard particles [18] revealed considerable differences between these types of materials. The flow velocity was controlled by the size of the outlet of the vertical cylindrical silo. The details of this setup are shown in the next section. Here, we extend that report by additional numerical simulations and focus on the internal velocity and stress fields.

*e-mail: ralf.stannarius@ovgu.de

2 Setup and materials

Figure 1 shows the experimental setup. It consists of a vertical cylinder of 14.4 cm inner diameter and 80 cm height. A spherical obstacle was placed 20 cm above the outlet, suspended by a thin wire. Load cells measured the force on the suspended ball and on the bottom plate.

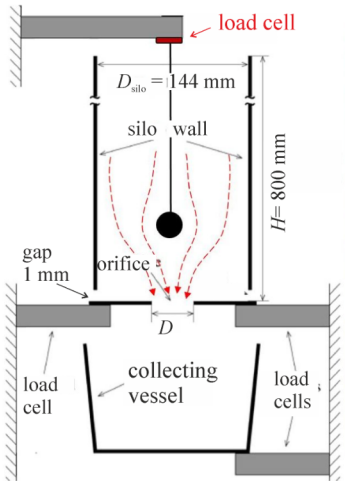

Figure 1. Schematic drawing of the silo setup with the suspended obstacle, the load cells and collecting vessel, including a crude sketch of the flow field. Obstacle diameters d_o were chosen between 10 mm and 40 mm. This setup was used for discharge experiments with soft, low-friction and hard, frictional grains [18].

The materials chosen were monodisperse hard glass spheres (GLS) of 3.15 mm diameter and soft, practically frictionless hydrogel spheres (HGS) of 7.5 mm diameter. They differ in both softness and friction coefficients. The separate consequences of these two parameters for silo discharge dynamics were studied by Pongó et al. [19]. They

found that the friction coefficient has only little influence on outflow rates for hard particles, yet low friction coefficients alter the outflow of soft grains considerably.

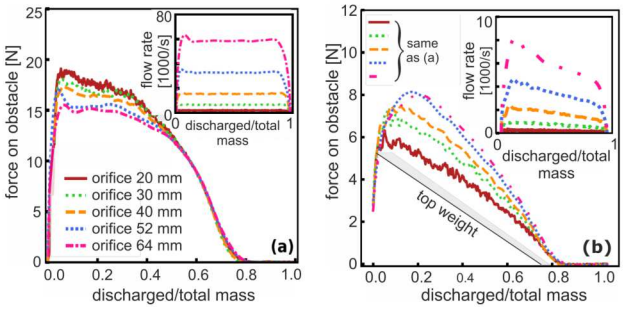

Figure 2. Forces on a spherical obstacle with diameter d_o = 40 mm in flowing GLS (a) and HGS (b) from experiments. Insets show the flow rates for the respective orifice widths D. The black line in (b) sketches the weight of the hydrogel material in a hypothetical column with the obstacle diameter above the ball. (adapted from Ref. [18]).

The outflow rates Q were varied by adjustment of the orifice diameter D between 20 and 64 mm, which resulted in a controlled variation of the outflow velocity by a factor of $\approx$ 30. The downward flow velocities v_0 near the obstacle are related to the outflow rate Q (in grains/s) by $v \approx 1.5 \cdot 10^{-3}$ mm $\cdot Q$ for the glass beads and $v \approx 2 \cdot 10^{-2}$ mm $\cdot Q$ for the hydrogels. Figure 2 shows experimental flow and force measurements. A comparison of the experimental data with numerical simulation results can be found in [18]. In GLS, Q is constant until the grain surface almost reaches the container bottom. In HGS, Q decreases noticeably with lower bed height, as observed earlier [20].

After filling, the ball is suspended force-free, not in a well-defined state. The discharge activates force chains and triggers a rapid increase of the force on the ball. Then, the ball in GLS experiences a force plateau until the granular surface approaches the ball. In HGS, a continuous decay of the force with lowering fill height is primarily the effect of the lower quasi-hydrostatic pressure acting on the ball's top [19]. For comparison, inertial drag of a liquid of comparable density and velocity would result in forces of a few mN only. The weight of the balls is negligible, but it was subtracted from the data nonetheless.

The 3D numerical setup mimics its experimental counterpart, with similar system and particle sizes, as well as particle properties. We perform DEM simulations using a Hertz-Mindlin contact model [21], computing the trajectories and contact forces. The most important simulation parameters are the Young moduli Y_{GLS} = 1.0 GPa and Y_{HGS} = 125 kPa, the normal restitution coefficients $e_{n,GLS}$ = 0.9 and $e_{n,HGS}$ = 0.5 and the friction coefficients μ_{GLS} = 0.5 and μ_{HGS} = 0.02). The material is incompressible (Poisson ratio 0.5). The particle-wall interaction parameters are similar to those of particle-particle interactions. Furthermore, we used a coarse-graining methodology [22], to access the relevant macroscopic fields of packing fraction $\phi(\vec{r})$, velocity $\vec{v}(\vec{r})$ and contact $\boldsymbol{\sigma}^c(\vec{r})$. and dynamic stress $\boldsymbol{\sigma}^k(\vec{r})$.

3 Results

While the flow rates varied by more than one order of magnitude, there was hardly an effect on the total drag of the glass beads. The force rather decreased slightly with stronger flow until it reaches a plateau. For the hydrogels, the opposite was found: stronger flow led to higher drag forces before before a plateau was reached [18]. More important was the observation that the force exerted by the slippery, soft HGS was roughly proportional to the ball's horizontal cross section area, whereas the force of the frictional GLS had much weaker dependence on the ball size, roughly linear in the diameter [18]. In order to understand the stress and flow field distributions inside the silo, results of numerical simulations are presented here. They provide information that is hardly accessible experimentally. In Figs. 3 to 6, data for given heights z and distances R from the central axis were averaged over all azimuthal angles in two-dimensional (R, z)-plots. Figure 3 shows the streamlines and absolute magnitude of flow in the silo. Except at the bottom, where the stagnant zone is narrower for hydrogels than for the hard spheres, the flow fields are comparable, differing only in magnitude. Thus, the assumption of equal geometrical conditions for both materials is justified. Figure 4 shows the local packing fraction, which for

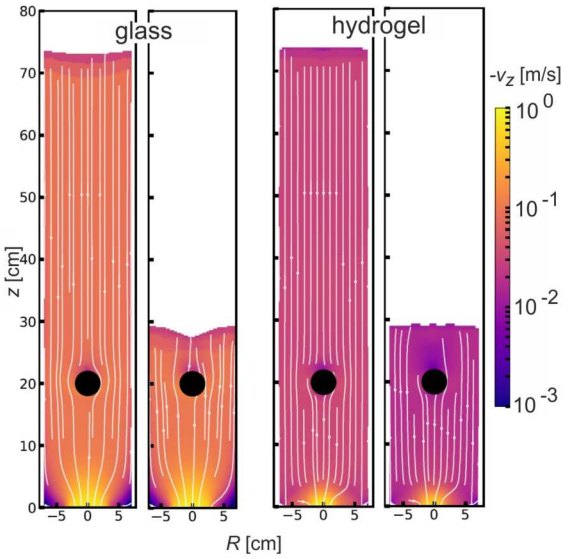

Figure 3. Simulated flow fields for GLS, 64 mm orifice (left) and HGS, 40 mm orifice (right). In both cases, streamlines are vertical and parallel except in the vicinity of the ball and the outlet. For HGS, the flow velocity reduces with lower fill levels. Snapshots are shown for 90% and 30% of the original fill height.

hard spheres is uniform, $\phi \approx 0.6$ (near random close packing, RCP), except near the outlet. The soft spheres pack much denser in the depth of the bed, since they deform for a more efficient space filling. When the pressure gradually reduces during the discharge, the packing expands towards RCP. This plot may also give a hint why the flow of HGS increases the drag force on the obstacle: The repeated inelastic compression and dilation of the soft spheres when they pass the obstacle dissipates energy, thus counteracting a quasi-frictionless shear flow. When the flow velocity

reaches a certain high level, this process saturates, presumably because the viscoelastic character of the hydrogels limits very fast shape relaxations. Figure 5 presents the

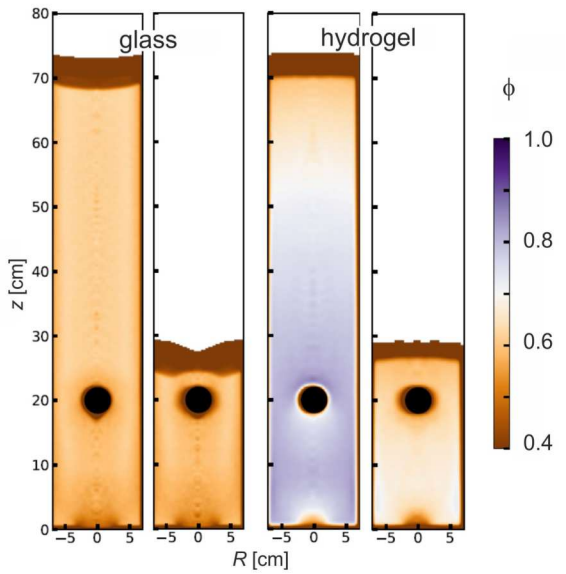

Figure 4. Simulated local packing fraction ϕ for GLS, $D = 64$ mm (left) and HGS, $D = 40$ mm (right). Snapshots at 90 % and 30 % of the original fill height. Deep in the HGS bed, the packing fraction is initially well above 80%, as the spheres are deformed by the pressure. When fill height and pressure get lower, ϕ approaches the RCP. The low packing in the very top layers is an averaging artifact.

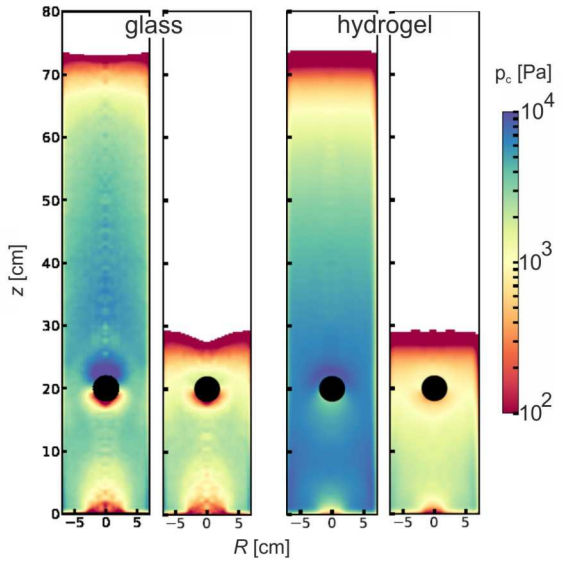

Figure 5. Simulated local contact pressure $p_c(r)$ for GLS (left) and HGS (right). Snapshots are shown for 90% and 30% of the original fill height. Note the focusing of the stress above the obstacle in GLS. The low stress in the very top layers is partially an averaging artifact.

profiles of contact pressure $p_c(r) = \mathrm{Tr}(\sigma^c(r))$ in the two materials. These plots probably reveal the most important insights into the difference between the two materials. In the soft HGS sample, the stress immediately above the obstacle is roughly uniform. The consequence is that the force acting on the ball is roughly proportional to the horizontal cross section. Moreover, a significant feature is that the stress below the obstacle, except for the region immediately below the ball, is comparable to the stress above. This means that the low-frictional soft material shows features which are closer to a liquid where the hydrostatic pressure below a submerged object is the same as without that object. On the other hand, the narrow zone of reduced stress below the obstacle is a consequence of the granular structure. It evidences that the forces acting on the bottom side of the ball are comparably weak, with a stress level approximately one order of magnitude below the one immediately above the ball. Thus, the "hydrostatic" net contribution to the force on the ball is not buoyancy, like in an ordinary liquid (where part of the pressure on the top surface is compensated by pressure from below), but rather this contribution equals the weight of the material on top. It is seen in Fig. 2 that the black line indicating the pressure on the upper hemisphere of the obstacle accounts for a large share of the total force experienced by the obstacle.

There is another qualitative difference: In HGS, the stress is almost independent of the distance from the central axis. Because of the low friction of the order of 10^{-2}, the walls carry only very little part of the HGS weight. In the case of the hard GLS material, there is a noticeable horizontal stress gradient in radial direction because of the much more efficient force transfer to the silo walls. Stress in the compartment below the obstacle is noticeably reduced in the GLS sample. The reason is that force chains redirect a substantial part of the grain weight above to the obstacle to the surface of that object.

In contrast to the low-frictional HGS sample, in GLS the stress on top of the obstacle is strongly focused in the center. This leads to a much weaker dependence of the net force on the upper surface area. Quantitatively, this has been described in more detail in [18].

Finally, we consider the kinetic stress $\sigma^k(r)$, which quantifies the local velocity fluctuations. Thus, its magnitude correlates with energy consumption rate due particle-particle collisions [22]. Figure 6 shows the calculated kinetic pressure profiles $p_k(r) = \mathrm{Tr}(\sigma^k(r))$ for GLS and HGS. While the region directly above the outlet naturally shows the largest velocity fluctuations and the shell around the obstacle is also characterized by stronger velocity fluctuations in both materials, the biggest difference is seen above the obstacle. There, the kinetic pressure of the soft HGS is an order of magnitude lower than that of the hard glass spheres. This indicates that the HGS material flows down rather like an *ordered dense flow* whereas in the flowing GLS, there is a *disordered collisional flow*, showing more micro-dynamics [23].

4 Summary

The force on a spherical obstacle suspended in granular material flowing downward during the discharge of a cylindrical container has been studied numerically as a function of the flow rate and the physical properties of the grains, complementing earlier experimental results.

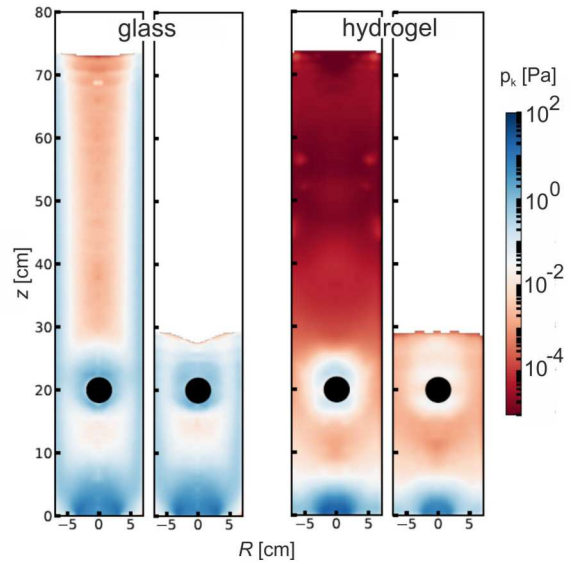

Figure 6. Simulated kinetic pressure $p_k(r)$ for GLS (left) and HGS (right). Snapshots are shown at 90% and 30% of the original fill height. In the hydrogels, the packing fraction is initially well above 80% deep in the granular bed, since the spheres are deformed by the pressure field. With lowering fill height, ϕ approaches the usual random close packing. The low packing in the top layers is an averaging artifact.

In rigid grains, the flow rate has only little influence on the force, whereas the soft hydrogels generate a velocity-dependent drag. We consider this a consequence of inelastic deformations of the soft grains when they pass the obstacle. The total force on the spherical obstacles in HGS is proportional to the horizontal obstacle cross section, which can be explained by the hydrostatic pressure on its top surface and negligible counter-forces from below. In the hard GLS, the pressure on the obstacle is strongly focused in the center [18], which leads to a much weaker, nearly linear radius dependence of the measured forces.

5 Acknowledgments

The authors acknowledge financial support by the European Union's Horizon 2020 program under the Marie Skłodowska-Curie ITN grant 812638, CALIPER. RC Hidalgo acknowledges financial support from the Spanish Government, through grant No. PID2023-146422NB-I00 (MICIU/AEI/10.13039/501100011033).

References

[1] L. Vanel et al., Memories in sand: Experimental tests of construction history on stress distributions under sandpiles, Phys. Rev. E **60**, R5040 (1999).

[2] J. Ai, J.Y. Ooi, J.F. Chen, J.M. Rotter, Z. Zhong, The role of deposition process on pressure dip formation underneath a granular pile, Mechanics of Materials **66**, 160 (2013).

[3] G.H.L. Hagen, Über den Druck und die Bewegung des trockenen Sandes, Bericht über die zur Bekanntmachung geeigneten Verhandlg. der Königl. Preuß. Akad. der Wissensch. zu Berlin p. 35 (1852).

[4] H.A. Janssen, Versuche über Getreidedruck in Silozellen, Zeitschr. d. Verein. dt. Ing. **39**, 1045 (1895).

[5] F. Zhou, S. Advani, E. Wetzel, Slow drag in granular materials under high pressure, Phys. Rev. E **69**, 061306 (2004).

[6] G. Hill, S. Yeung, S.A. Koehler, Scaling vertical drag forces in granular media, Europhys. Lett. **72**, 137 (2005).

[7] M. B. Stone et al., Local jamming via penetration of a granular medium, Phys. Rev. E **70**, 041301 (2004).

[8] T.A. Brzinski, P. Mayor, D.J. Durian, Depth-dependent resistance of granular media to vertical penetration, Phys. Rev. Lett. **111**, 168002 (2013).

[9] W. Kang, Y. Feng, C. Liu, R. Blumenfeld, Archimedes' law explains penetration of solids into granular media, Nature Comm. **9**, 1101 (2018).

[10] T. Hossain, P. Rognon, Rate-dependent drag instability in granular materials, Granular Matter **22**, 72 (2020).

[11] L.K. Roth, Constant speed penetration into granular materials: drag forces from the quasistatic to inertial regime, Granular Matter **23**, 54 (2021).

[12] H. Tsunakawa, R. Aoki, The vertical force of bulk solids on objects in bins, Powder Technology **11**, 237 (1975).

[13] T. Atkinson, J. Butcher, M. Izard, R. Nedderman, The forces on obstacles suspended in flowing granular materials, Chem. Eng. Sci. **38**, 91 (1983).

[14] D. Chehata, R. Zenit, C. Wassgren, Dense granular flow around an immersed cylinder, Phys. Fluids **15**, 1622 (2003).

[15] P. Moysey, N. Rao, M. Baird, Dynamic coefficient of friction and granular drag force in dense particle flows: Experiments and DEM simulations, Powder Technology **248**, 54 (2013).

[16] R. Kobylka, M. Molenda, J. Horabik, Loads on grain silo insert discs, cones, and cylinders: Experiment and DEM analysis, Powder Technology **343**, 521 (2019).

[17] N. Coppin, M. Constant, J. Lambrechts, F. Dubois, V. Legat, Numerical analysis of the drag on a rigid body in an immersed granular flow, Comp. Particle Mech. **9**, 393 (2022).

[18] J. Wang et al., Force on a sphere suspended in flowing granulate, Phys. Rev. E **108**, L062901 (2023).

[19] T. Pongó et al., Flow in an hourglass: particle friction and stiffness matter, New J. Phys. **23**, 023001 (2021).

[20] K. Harth, J. Wang, T. Börzsönyi, Intermittent flow and transient congestions of soft spheres passing narrow orifices, Soft Matter **16**, 8013 (2020).

[21] T. Pöschel, T. Schwager, Computational Granular Dynamics (Springer-Verlag, 2005)

[22] I. Goldhirsch, Stress, stress asymmetry and couple stress: from discrete particles to continuous fields, Granular Matter **12**, 239 (2010).

[23] P. Rognon, M. Macaulay, Shear-induced diffusion in dense granular fluids, Soft Matter **17**, 5271 (2021).